A&A 510, A42 (2010)
DOI: 10.1051/0004-6361/200913052

Astronomy & Astrophysics

The ATESP 5 GHz radio survey

III. 4.8, 8.6 and 19 GHz follow-up observations of radio galaxies

I. Prandoni[1], H. R. de Ruiter[1], R. Ricci[1,2], P. Parma[1], L. Gregorini[3,1], and R. D. Ekers[4]

[1] INAF - Istituto di Radioastronomia, via Gobetti 101, 40129 Bologna, Italy
e-mail: i.prandoni@ira.inaf.it
[2] Department of Physics and Astronomy, University of Calgary, 2500 University Drive NW, Calgary, AB T2N 1N4, Canada
[3] Dipartimento di Astronomia, Università di Bologna, via Ranzani 1, 40127 Bologna, Italy
[4] Australia Telescope National Facility, CSIRO, PO Box 76, Epping NSW 1710, Australia

Received 2 August 2009 / Accepted 3 November 2009

ABSTRACT

Aims. Physical and evolutionary properties of the sub-mJy radio population are not entirely known. The radio/optical analysis of the ATESP 5 GHz sample has revealed a significant class of compact flat/inverted radio-spectrum sources associated to early-type galaxies up to redshift 2. Such sources are most plausibly triggered by an AGN, but their observational properties are not entirely consistent with those of standard radio galaxy populations. In the present work we aim at a better understanding of the radio spectra of such sources and ultimately of the nature of AGNs at sub-mJy flux levels. In particular we are interested in assessing whether the AGN component of the sub-mJy population is more related to efficiently accreting systems – like radio-intermediate/quiet quasars – or to systems with low accretion rates – like e.g. FRI radio galaxies – or to low radiative efficiency accretion flows – like e.g. ADAF.
Methods. We used the ATCA to get multi-frequency (4.8, 8.6 and 19 GHz) quasi-simultaneous observations for a representative sub-sample of ATESP radio sources associated with early-type galaxies (26 objects with $S > 0.6$ mJy). This can give us insight into the accretion/radiative mechanism that is at work, since different regimes display different spectral signatures in the radio domain.
Results. From the analysis of the radio spectra, we find that our sources are most probably jet-dominated systems. ADAF models are ruled out by the high frequency data, while ADAF+jet scenarios are still consistent with flat/moderately inverted-spectrum sources, but are not required to explain the data. We compared our sample with high (≳20 GHz) frequency selected surveys, finding spectral properties very similar to the ones of much brighter ($S > 500$ mJy) radio galaxies extracted from the Massardi et al. (2008) sample. Linear sizes of ATESP 5 GHz sources associated with early type galaxies are also often consistent with the ones of brighter B2 and 3C radio galaxies, with possibly a very compact component that could be associated at least in part to (obscured) radio-quiet quasar-like objects and/or low power BL Lacs.

Key words. surveys – radio continuum: general – methods: data analysis – catalogs – galaxies: general – galaxies: evolution

1. Introduction

After many years of studies, AGNs are now recognised to contribute significantly at radio fluxes below 1 milliJy (mJy). Multi-wavelength studies of deep radio fields show that star-forming galaxies dominate at microJy (μJy) levels (Richards et al. 1999), while radio sources associated with early-type galaxies and plausibly triggered by AGNs, are the most significant source component (~60–70% of the total) at higher flux densities (>100–200 μJy) with a further 10% contribution from broad-/narrow-line AGNs (see e.g. Gruppioni et al. 1999; Georgakakis et al. 1999; Magliocchetti et al. 2000; Prandoni et al. 2001b; Muxlow et al. 2005; Afonso et al. 2006; Mignano et al. 2008; Smolcic et al. 2008). This somehow unexpected presence of large numbers of AGN-type sources at the sub-mJy level has given a new and interesting scientific perspective to the study of deep radio fields, since a better understanding of the physical and evolutionary properties of such low/intermediate power AGNs may have important implications for the determination of the black-hole-accretion history of the Universe as derived from radio-selected samples. Of particular interest is the possibility of assessing whether the AGN component of the sub-mJy population is more related to efficiently accreting systems – like radio-intermediate/quiet quasars – or to systems with very low accretion rates – like e.g. FRI radio galaxies (Fanaroff & Riley 1974). The latter scenario (radio mode) is supported by the presence of many optically inactive early type galaxies among the sub-mJy radio sources. The quasar mode scenario, on the other hand, may be supported by the large number of so-called radio-intermediate quasars observed at mJy levels (see e.g. Lacy et al. 2001) and by the modelling work of Jarvis & Rawlings (2004), who predict a significant contribution of radio-quiet quasars at sub-mJy levels. Another issue is represented by the possible role played at low radio fluxes by low radiation efficiency accretion mechanisms, associated to optically thin discs, such as the so-called *advection dominated accretion flows* (ADAF) and modifications (ADIOS, CDAF, etc; see Narayan & Yi 1994; Quataert & Narayan 1999; Abramowitcz et al. 2002).

One especially suited radio sample to study the phenomenon of low-luminosity nuclear activity, possibly related to low radiation/accretion processes and/or radio-intermediate/quiet QSOs, is the so-called ATESP 5 GHz survey, carried out with the

Australia Telescope Compact Array (ATCA) by Prandoni et al. (2006), which covers a 2×0.5 sq. deg region of the wider original 1.4 GHz ATESP survey (Prandoni et al. 2000a,b, 2001a). In the region of the ATESP 5 GHz survey we have 131 radio sources with flux densities larger than $S \sim 0.4$ mJy detected either at 1.4 GHz or 5 GHz or both. Interestingly, the analysis of the 1.4 and 5 GHz ATESP data has revealed a significant flattening of the source radio spectra going from mJy to sub-mJy flux levels (Prandoni et al. 2006). Such flattening is mostly associated to early-type galaxies as demonstrated by deep ($R < 25$) *UBVRIJK* multi-colour imaging. At the flux limit of the sample star-forming galaxies are starting to appear, but are not yet the dominant population: ∼14% of the sources are identified with broad/narrow-line AGNs and another ∼64% is identified with early-type galaxies, most probably triggered by an AGN (see Mignano et al. 2008). The absence of emission lines in the latter together with low radio luminosities (typically 10^{22-25} W/Hz) suggests that these are FRI radio galaxies. However, >60% of them show flat ($\alpha > -0.5$, where $S \sim \nu^{\alpha}$) and/or inverted ($\alpha > 0$) spectra and rather compact linear sizes ($d < 10-30$ kpc, see Mignano et al. 2008). Both compactness and spectral shape suggest a core emission with strong synchrotron or free-free self-absorption. Such sources are known to exist among FRI radio galaxies, but they are relatively rare. It is therefore important to confirm the existence of such a large class of flat/inverted spectrum objects through simultaneous radio observations at different radio wavelengths.

If real, these sources may represent a composite class of objects very similar to the so-called low power ($P_{408\ \mathrm{MHz}} < 10^{25.5}$ W/Hz) compact (<10 kpc) – LPC – radio sources studied by Giroletti et al. (2005). LPC host galaxies do not show signatures of strong nuclear activity in the optical (and X-ray) bands, and preliminary results indicate that multiple causes can produce LPC sources: geometrical-relativistic effects (low power BL-Lacertae objects), youth (GPS-like sources), instabilities in the jets, frustration by a denser than average ISM and a premature end of nuclear activity (sources characterised by low accretion/radiative efficiency, i.e. ADAF/ADIOS systems). Some difficulties remain however. First, if the objects are young GPS sources, much higher (>10^{25} W/Hz) radio luminosities are expected; second, if they are old ADAF/ADIOS sources, the expected luminosities are much lower (<10^{21} W/Hz, Doi et al. 2005). In the latter case there may yet be different solutions, as for example if the ADAF source coexists with a radio jet, as was suggested by Doi et al. (2005) in the case of a few low luminosity AGNs (see also the ADAF-jet model of Falcke & Biermann 1999).

Another possibility is that we are dealing with radio-quiet/intermediate QSOs, where the activity in the optical band is obscured by dust in the galaxy. This scenario may be supported by the results reported by Klöckner et al. (2009), who have recently observed with the EVN 11 $z > 2$ radio-intermediate obscured quasars (several with flat-spectrum), detecting seven of them. The detected radio emission accounts for 30−100% of the entire source flux density, and the physical extent of this emission is $\lesssim$150 pc. The missing flux implies the likely existence of radio jets of physical sizes between $\gtrsim$150 pc and $\lesssim$40 kpc.

The aim of the present paper is a better understanding of the physical properties of the AGNs associated to early-type galaxies in the ATESP 5 GHz sample. The study of the radio spectra, based on multi-wavelength (simultaneous) observations, is essential in this respect, since different source types (e.g. GPS vs. BL Lac) and/or accretion scenarios (e.g. jet-dominated vs. ADAF/ADIOS-dominated) lead to different shapes of the radio spectrum. Particularly useful is the availability of high radio frequency information, since, for example the location of the frequency at which the radio spectrum peaks may be an indication of the presence or absence of outflows. A pure ADAF model without outflow is expected to peak in the sub-mm regime (the "sub-mm bump") and has an inverted ($\alpha > 0$) spectrum in the cm range (see e.g. Nagar et al. 2001). As outflows become important, the peak shifts to longer wavelengths (above 1 cm), and depending on which frequencies were observed, the spectra might be classified as flat ($\alpha > -0.5$) or steep ($\alpha < -0.5$).

In this paper we report on quasi-simultaneous observations at 4.8, 8.6 and 19 GHz of a subset of ATESP 5 GHz sources associated to early-type galaxies. Our results will be compared to the ones obtained by new high frequency (>10 GHz) radio surveys. Such surveys have started only recently, notably with the ATCA at 20 GHz (Ricci et al. 2004; Sadler et al. 2006; Massardi et al. 2008), and detailed spectral studies based on high radio frequency observations are therefore still scarce. Other deeper recent high frequency surveys are the one by Tucci et al. (2008), who observed sources with $S > 20$ mJy at 33 GHz and compared the composition of the source counts with the high frequency model counts of De Zotti et al. (2005), and the 9C survey at 15 GHz (a 124 source sample complete to 25 mJy and a 70 source sample complete to 60 mJy, Bolton et al. 2004). In the latter case the observed source counts were discussed in Waldram et al. (2007). The data presented in this paper represent the first high frequency (>10 GHz) systematic follow-up of a sample of sub-mJy radio sources.

The paper is organized as follows. We discuss the selection of the sample, the follow-up observations at 4.8, 8.6 and 19 GHz and the data reduction in Sects. 2 and 3; source variability at 4.8 GHz (where data at two epochs are available) is discussed in Sect. 4; a complete discussion of the radio spectra, in comparison with high-frequency selected samples, is given in Sect. 5. A further comparison with (FRI and FRII) radio galaxies and radio-quiet QSOs is presented in Sect. 6, where we discuss source linear sizes and radio powers. A brief summary of the main results of this work is given in Sect. 7. Throughout this paper we use the ΛCDM model, with $H_0 = 70$, $\Omega_{\mathrm{m}} = 0.3$ and $\Omega_{\Lambda} = 0.7$.

2. Sample selection

In order to better assess the composite nature of the sub-mJy population with particular respect to the low-/intermediate-luminosity AGN component, we are studying in great detail a sample of 131 sources with $S > 0.4$ mJy distributed over a 2×0.5 square degree region in the southern sky surveyed at both 1.4 and 5 GHz in the framework of the ATESP 1.4 and 5 GHz radio surveys (Prandoni et al. 2000a,b, 2001a, 2006). This region overlaps entirely with the so-called "Deep1" sub-region of the ESO *Deep Public Survey* (DPS) survey (Mignano et al. 2007; Olsen et al. 2006). As described in detail in Mignano et al. (2007), deep ($R < 25$), multi-colour (*UBVRIJK*) optical/NIR data have been collected for a part of this region (1×0.5 sq. deg, namely fields Deep1a, and b) in the framework of the DPS and for another part (0.5×0.5 sq. deg, namely field Deep1c) in the framework of the Garching-Bonn Deep Survey (GaBoDS, Hildebrandt et al. 2006), allowing us to derive photometric redshifts and types for virtually all the radio sources optically identified down to $I < 23.5$ in this region (Mignano et al. 2008). Such data are complemented in the remaining 0.5×0.5 sq. deg field (Deep1d) by shallower optical imaging ($I < 22.5$) obtained in the framework of the ESO public survey EIS-WIDE (Nonino et al. 1999)

Table 1. ATESP-Deep1 sample: statistics.

Deep1	Total sample			*Bright* sample ($S \geq 0.6$ mJy)			C/X, K band Follow-up	
	N_S	$N_S^{\rm opt}$	N_S^E	N_S	$N_S^{\rm opt}$	N_S^E	N_S^E	$N_S^{\neq E}$ [a]
a, b, c	85	56	37	48	32	23	23	3[b]
d	46	15	10	31	9	5	3[c]	–
All	131	71	47	79	41	28	26	3

[a] Sources for which a preliminary early-type classification has not been confirmed; [b] J225048-400147; J225321-402317; J225504-400154; [c] J224516-401807; J224547-400324; J224654-400107.

and shallower spectroscopic information ($b_j < 19.4$, Vettolani et al. 1998; $I < 19$, Prandoni et al. 2001b; $I < 21.5$ Prandoni et al., in prep.). This means that in field Deep1d optical identification and spectral classification is available only for ∼33% of the radio sources.

For the purposes of this work we are interested in the sources identified with early type galaxies. As reported in Table 1 (Cols. (2)−(4)), we have 85 radio sources in fields Deep1a,b,c, 56 of which have been optically identified and spectrally classified ($I < 23.5$); 37 of these sources (27 having flat/inverted spectra) are associated to early-type galaxies. To these sources we can add another 15 (out of 46) sources optically identified and spectrally classified in field Deep1d, ten of which are associated to early type galaxies (five with flat/inverted spectrum).

Subsequently we will focus our analysis on a *bright* sub-sample: for sensitivity reasons we limited our multi-frequency (4.8, 8.6 and 19 GHz) follow-up to radio sources with S(5 GHz) ≥ 0.6 mJy. We have a total of 79 such sources (48 in fields Deep1a,b,c plus 31 in field Deep1d), 41 (32 + 9) having an optical spectral classification and 28 (23 + 5) being classified as early-type (see Table 1, Cols. (5)−(7)). For the 6/3 cm and 12 mm follow-up (see Table 1, Cols. (8), (9)) we gave priority to the 23 sources in fields Deep1a,b,c, whose optical identification is virtually complete down to $I \sim 23.5$. Nevertheless multi-frequency (6/3 cm and 12 mm) quasi-simultaneuous observations have been undertaken also for a sub-set of three (out of five) Deep1d sources and for three radio sources in fields Deep1a,b,c, which were preliminarly classified as early-type at the time of the 2007 observations, but not confirmed as such in the final optical analysis (see Mignano et al. 2008).

We notice that no target selection was done based upon the source radio spectral shape. In other words, both flat/inverted and steep spectrum sources were observed. A comparison between flat, inverted and steep sources is important to either assess the possibly composite AGN component of the faint radio population, or to test for various accretion models, from pure ADAF to ADAF+outflows/jets to pure jet-related accretion.

We also notice that repeating the 5 GHz observations (already available from the ATESP 5 GHz survey) allows us to test the importance of variability in the present sample (see Sect. 4).

3. Radio observations and data reduction

3.1. Observations

The 4.8, 8.6 and 19 GHz observations were carried out in two separate campaigns in 2007 (15 sources) and 2008 (14 sources) with the ATCA. The expected flux densities at 8.6 and 19 GHz were computed based upon the source flux densities at 5 GHz and the spectral index between 1.4 and 5 GHz (obtained from the original ATESP 1.4 and 5 GHz surveys, Prandoni et al. 2000b, 2006). From the expected flux densities, sensitivity and total time to be spent on source were derived by requesting at least a $S/N = 6$.

Table 2. Follow-up source list observed in May 2007.

source name	RA (J2000)	Dec (J2000)	$t_{C/X}$ (min)	t_K (min)
J225034-401936	22 50 34.61	–40 19 36.3	5.0	4.0
J225048-400147	22 50 48.04	–40 01 47.0	22.5	10.0
J225057-401522	22 50 57.79	–40 15 22.5	7.5	6.0
J225223-401841	22 52 23.82	–40 18 41.9	47.5	42.0
J225249-401256	22 52 49.92	–40 12 56.0	35.0	40.0
J225321-402317	22 53 21.28	–40 23 17.7	35.0	62.5
J225322-401931	22 53 22.73	–40 19 31.6	50.0	82.0
J225323-400453	22 53 23.89	–40 04 53.7	30.0	10.0
J225344-401928	22 53 44.89	–40 19 28.6	167.5	180.0
J225404-402226	22 54 04.33	–40 22 26.9	5.0	14.0
J225430-400334	22 54 30.47	–40 03 34.0	50.0	8.0
J225434-401343	22 54 34.70	–40 13 43.2	5.0	4.0
J225436-400531	22 54 36.29	–40 05 31.3	67.5	38.0
J225449-400918	22 54 49.73	–40 09 18.6	55.0	66.0
J225504-400154	22 55 04.67	–40 01 54.8	5.0	6.0

Table 2 shows the list of 15 sources observed in 2007 with target positions and observing times for the C/X band and the K-band observations respectively. The 4.8 and 8.6 GHz observations were conducted on April 30th, May 1st and 6th 2007. Both frequencies were observed simultaneously with a bandwidth of 128 MHz. The ATCA operated in the 1.5C array configuration, which gives an angular resolution at 5 GHz comparable to the one of the original ATESP 1.4 GHz 6-km ATCA configuration (10−15 arcsec). This is important since we want to derive spectral indices from source flux measurements. Nevertheless we include the 6-km antenna in the observations in order to be able to perform a higher resolution analysis of the source structure. Each source received an average of five linear cuts on a range of hour angles between $-4^{\rm h}$ and $+1^{\rm h}$ in order to maximize the (u, v) plane coverage. A phase calibrator was observed every 20−25 min in 1-min scans. The K-band observations were carried out on May 25th and 26th 2007 on the same list of sources observed at 4.8 and 8.6 GHz at two simultaneous IFs (Intermediate Frequencies), i.e. at 18.496 and 19.520 GHz. The band-width of both IFs was 128 MHz. The total observing time on source is reported in Table 2. The array configuration was H214: a hybrid and shorter array configuration was chosen in order to map the sources with a smaller number of cuts (snapshots) and with an angular resolution (10−15 arcsec) roughly matching the one used for the 4.8/8.6 GHz observations. Again the 6-km antenna was included in the observations. Each target source was scanned for a total of four times during the two-day run in a HA range of $1^{\rm h}$ to $4^{\rm h}$.

The list of 14 targets observed in 2008 with the source positions and integration times is given in Table 3. The C- and X-band run was carried out in a single day on July 7th 2008 with the ATCA in the array configuration 1.5B. An average of seven scans was collected for each target source in HA range $-6^{\rm h}$ – $+4^{\rm h}$. The K-band run was scheduled on July 11th and 12th 2008 in two three-hour sessions with the same frequency setting and configuration used in 2007. A total number of four cuts in the HA range $1^{\rm h} - 3^{\rm h}.5$ was collected for each target during the two observing sessions. The 6-km antenna was included also for the 2008 observing runs.

Table 3. Follow-up source list observed in July 2008.

source name	RA (J2000)	Dec (J2000)	$t_{C/X}$ (min)	t_K (min)
J224516-401807	22 45 16.70	–40 18 07.8	7.0	4.0
J224547-400324	22 45 47.88	–40 03 24.2	7.0	2.0
J224654-400107	22 46 54.53	–40 01 07.2	7.0	2.0
J224750-400148	22 47 50.03	–40 01 48.6	7.0	2.0
J224753-400455	22 47 53.73	–40 04 55.1	210.0	140.0
J224822-401808	22 48 22.12	–40 18 08.2	7.0	2.0
J224827-402515	22 48 27.20	–40 25 15.7	42.0	4.0
J224919-400037	22 49 19.35	–40 00 37.2	105.0	28.0
J224935-400816	22 49 35.21	–40 08 16.9	42.0	6.0
J224958-395855	22 49 58.26	–39 58 55.4	14.0	2.0
J225004-402412	22 50 04.43	–40 24 12.4	21.0	6.0
J225008-400425	22 50 08.82	–40 04 25.5	21.0	6.0
J225239-401949	22 52 39.29	–40 19 49.5	42.0	16.0
J225529-401101	22 55 29.51	–40 11 01.7	35.0	8.0

3.2. Data reduction

The raw visibility data were reduced using the astronomical software package MIRIAD (Sault et al. 1995). The data were read into MIRIAD, checked, flagged and split into single-source single-frequency files. The bandpass was equalised using the standard ATCA calibrator 1921-293 (apart from 2007 K-band run where 2243-123 was used instead). The absolute flux scale was bootstrapped using the standard ATCA primary calibrator 1934-638. The phase calibrators 2226-411 and 2232-488 (only for the 2008 K-band run) were used to solve for the amplitude and phase complex gains in each observing frequency. The calibrated visibilities were then imaged by Fourier inversion, *after excluding the 6-km antenna*: the 4.8 and 8.6 GHz visibilities were imaged separately. The K-band visibilities were instead combined into a single 19-GHz image by using the Multi Frequency Synthesis (MFS) technique (Sault & Wieringa 1994). In the case that the observing frequencies of two or more IFs are not too far apart so that radio spectral shape effects are still negligible, the MFS technique can be used effectively to increase the (u, v) plane coverage and minimise the band-width smearing effects and thus improve the final image quality. As we were carring out a detection experiment, inverted images were inspected using the KARMA package visualisation tool *kvis* to search for at least a 3-sigma detection in the inverted image position were the source was expected to be found (the field centre). In case of detection the source images were cleaned and restored using standard clean algorithms: Högbom (1974), Clark (1980) or Steer (Steer et al. 1984). The MFS technique was used only at the Fourier inversion stage, *not* at the cleaning stage.

Limited (u, v) angle coverage of the C/X band observations produced elongated restoring beams ($24'' \times 6''$ at 4.8 GHz and $14'' \times 3.5''$ at 8.6 GHz in 2007; $18'' \times 7''$ at 4.8 GHz and $10'' \times 4''$ at 8.6 GHz in 2008), making the cleaning unreliable. We therefore decided to determine the source fluxes by directly fitting a Gaussian point-like model to the calibrated visibilities. In order to check for the presence of extended structure, we fitted the visibilities at different angular resolutions. We compared the fluxes obtained by either including or removing the 6-km antenna, or, for the 8.6 GHz observations only, by removing all baselines longer than 750 m (corresponding to 25 $k\lambda$) in order to have a similar angular resolution as for the 4.8 GHz observations ($20'' \times 6''$).

From this analysis we found that most of the sources are detected ($S/N \geq 3$) at either 4.8 or 8.6 GHz or both, and that most of the detected sources can be reliably considered point-like at the lowest angular resolution (no 6-km antenna at 4.8 GHz and no baselines longer than 750 m at 8.6 GHz). For those sources (peak) flux densities were determined by fitting a point-like Gaussian to the lowest resolution datasets. The remaining sources (typically well-resolved or multi-component in the original ATESP 5 GHz catalogue, Prandoni et al. 2006) were uv-fitted with a single Gaussian whenever suitable, or were alternatively fitted with multi-component Gaussians in the restored images (convolved to the same resolution as for the other frequencies). For such resolved sources integrated flux densities were considered to derive the spectral index.

The (u, v) plane coverage obtained for the K-band observations is much better, thanks to the availability of north-south baselines of the hybrid ATCA configuration (restoring beam $\sim 10'' \times 8''$, excluding the 6-km antenna). Therefore K-band flux densities were derived by performing source Gaussian fitting in the image plane. Peak (or integrated) flux densities were used for unresolved (or resolved) sources to derive the spectral index.

For all undetected sources 3σ upper limits were derived by estimating the noise from V Stokes parameter visibilities for the C/X band observations and directly from the images for K-band observations.

In Table 4 we summarise the flux densities at the available four frequencies for all the 29 sources observed. The three sources not identified with early type galaxies (see discussion in Sect. 2) are explicitely indicated in the table. For the new observations we list also the rms noise values estimated directly from the images (for K-band observations) or from V Stokes parameter visibilities (for C/X observations). ATESP observations were designed to have very uniform image rms values of the order of 0.08–0.09 mJy at 1.4 GHz and 0.06–0.08 mJy at 5 GHz (Prandoni et al. 2000a, 2006). The rms noise values can be used to estimate source signal-to-noise ratios and uncertainties in the flux density measurements. Table 4 also lists $\alpha_{\rm L}$ and $\alpha_{\rm H}$, the spectral indices derived at low and high frequency respectively. In particular we used the original ATESP 1.4 and 5 GHz flux densities to derive $\alpha_{\rm L}$ and the new simultaneous 8.6 and 19 GHz measurements to derive $\alpha_{\rm H}$. We notice however that for sources undetected at 8.6 GHz, $\alpha_{\rm H}$ was derived by using the simultaneous 4.8 GHz flux measurement, if available. Radio spectra and contour plots for the 26 sources associated to early-type galaxies are presented later in the paper in Figs. 4 and 7.

Figure 1 compares the ATESP 5 GHz fluxes (Prandoni et al. 2006) with the 5 GHz fluxes obtained from the multi-frequency observation campaign presented here. The two epoch fluxes agree reasonably well with larger scatters for fainter sources (generally corresponding to lower signal-to-noise ratios). The highest deviations from the expected 1:1 line at high flux levels are found for multiple/extended sources (circled dots) where new integrated flux determinations, based on poor (u, v)-angle coverage data, may be underestimated due to the presence of undetected low surface brightness extended flux. In Sect. 4 we will also explore the possible role of source variablity in producing significant 5 GHz flux deviations in single-component sources.

3.3. Full resolution K-band imaging

ATESP 5 GHz sources were originally imaged at both low ($\sim 10''$) and full ($\sim 2''$) resolution (Prandoni et al. 2006), in order to study their structure (see contours in Fig. 7). Here we exploit the K-band data to repeat this kind of analysis at a higher frequency. K-band images were produced at full resolution ($\sim 2''$) by including the 6-km antenna in the imaging and cleaning

Table 4. Flux densities and spectral indices of ATESP-Deep1 sample.

Source	ATESP flux		2007/2008 Flux and rms noise values						Spectral indices	
	20 cm (mJy)	6 cm (mJy)	6 cm (mJy)		3 cm (mJy)		1.2 cm (mJy)		α_L	α_H
J224516-401807	9.54	3.87	3.30	0.24	<1.44	0.48	<0.57	0.19	–0.71 ± 0.04	<–1.28
J224547-400324	32.83	28.28	30.49	0.42	26.64	0.60	27.89	0.84	–0.12 ± 0.01	0.06 ± 0.01
J224654-400107	5.59	3.15	<1.26	1.00	<1.44	0.48	1.11	0.26	–0.45 ± 0.05	–
J224750-400148	13.44	6.09	5.22	0.23	2.63	0.17	0.98	0.30	–0.62 ± 0.02	–1.25 ± 0.29
J224753-400455	2.08	0.67	1.15	0.08	0.43	0.11	0.27	0.06	–0.89 ± 0.19	–0.59 ± 0.34
J224822-401808	19.08	10.34	10.04	0.42	7.29	0.61	4.24	0.31	–0.48 ± 0.01	–0.69 ± 0.04
J224827-402515	0.58	0.80	0.51	0.17	1.12	0.25	<0.78	0.26	0.25 ± 0.27	<–0.46
J224919-400037	0.91	0.64	<0.33	0.11	0.69	0.16	0.43	0.10	–0.28 ± 0.23	–0.60 ± 0.32
J224935-400816	0.70	0.82	1.02	0.29	<0.57	0.19	<0.60	0.20	0.12 ± 0.23	<–0.39
J224958-395855	1.52	1.65	<0.90	0.30	<1.02	0.34	1.52	0.34	0.06 ± 0.12	–
J225004-402412	3.16	1.78	1.89	0.24	<0.84	0.28	1.28	0.21	–0.45 ± 0.08	–0.28 ± 0.07
J225008-400425	2.88	1.70	1.61	0.39	<0.84	0.28	<0.66	0.22	–0.41 ± 0.09	<–0.65
J225034-401936	76.62	25.78	21.16	0.30	17.20	0.85	6.03	0.33	–0.86 ± 0.01	–1.33 ± 0.02
J225048-400147([a])	0.60	0.96	0.76	0.17	1.13	0.23	<0.51	0.17	0.37 ± 0.27	<–1.01
J225057-401522	2.01	3.00	3.44	0.29	2.16	0.40	2.51	0.28	0.31 ± 0.08	0.19 ± 0.14
J225223-401841	0.98	0.85	0.55	0.12	<0.51	0.17	0.46	0.13	–0.11 ± 0.20	–0.13 ± 0.21
J225239-401949	2.26	1.18	1.71	0.30	1.02	0.25	<0.42	0.14	–0.51 ± 0.12	<–1.13
J225249-401256	1.52	1.09	0.93	0.15	0.84	0.21	0.71	0.10	–0.26 ± 0.14	–0.21 ± 0.24
J225321-402317([a])	2.32	1.21	1.31	0.11	<0.57	0.19	0.31	0.09	–0.51 ± 0.11	–1.05 ± 0.15
J225322-401931	1.86	1.01	0.96	0.12	0.92	0.17	0.43	0.09	–0.48 ± 0.14	–1.06 ± 0.23
J225323-400453	0.51	0.85	0.53	0.16	<0.69	0.23	0.75	0.23	0.40 ± 0.31	0.25 ± 0.31
J225344-401928	0.60	3.52	1.76	0.10	2.12	0.14	2.05	0.08	1.39 ± 0.25	–0.04 ± 0.02
J225404-402226	10.34	3.80	3.08	0.43	3.79	0.64	0.78	0.21	–0.79 ± 0.03	–2.01 ± 0.30
J225430-400334	<0.26	0.63	<0.42	0.14	1.43	0.20	1.26	0.29	>0.70	–0.16 ± 0.21
J225434-401343	21.09	7.80	4.78	0.44	2.95	0.64	2.67	0.43	–0.78 ± 0.01	–0.13 ± 0.21
J225436-400531	0.47	0.60	0.90	0.14	0.54	0.15	<0.45	0.15	0.19 ± 0.36	<–0.23
J225449-400918	1.24	0.86	0.95	0.15	0.53	0.16	<0.36	0.12	–0.29 ± 0.17	<–0.49
J225504-400154([a])	9.67	4.59	4.97	0.92	4.91	1.53	<1.17	0.39	–0.59 ± 0.03	<–1.82
J225529-401101	1.48	1.09	1.32	0.19	1.34	0.27	<0.63	0.21	–0.24 ± 0.14	<–0.96

([a]) Sources not identified with early-type galaxies.

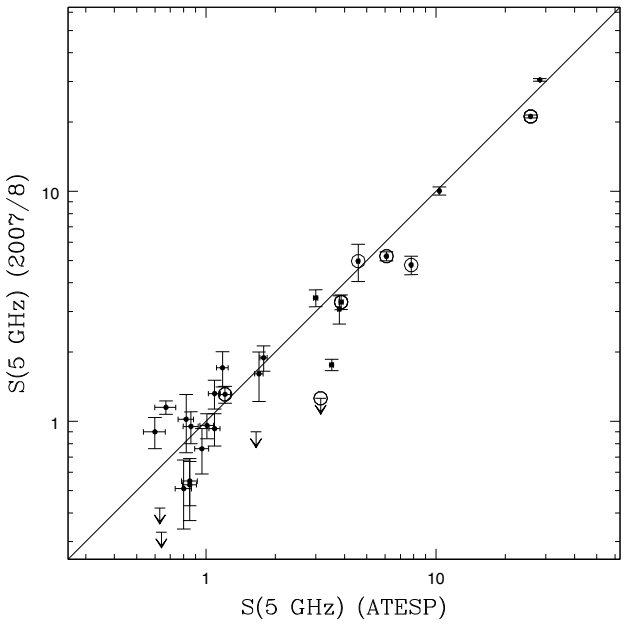

Fig. 1. Comparison between ATESP 5 GHz fluxes and new 5 GHz flux measurements obtained in 2007/2008. Upper limits are shown as downwards arrows. Multi-component an/or non-Gaussian extended sources are circled. The solid line represents S(ATESP) = S(2007/2008).

process. This has been done for all sources detected in K-band low resolution images with $S/N > 6$ (7 in total). Results are reported in Table 5 and Fig. 2, where K-band contour plots at low (thin contours) and full (thick contours) resolution are shown. Unfortunately the full resolution K-band imaging does not provide clear morphological information for any source, except for the source J224547-400324, which shows an elongated structure in east-west direction.

Table 5. Full resolution K-band imaging. Source parameters.

Source name	RA (J2000)	Dec (J2000)	$S_{int} \pm 1\sigma$ (mJy)
J224547-400324	22 45 47.67	–40 03 23.4	25.70 ± 0.22
J224822-401808([a])	22 48 21.99	–40 18 07.8	3.22 ± 0.24
J225004-402412([b])			1.70 ± 0.20
J225034-401936([b])			7.15 ± 0.31
J225057-401522	22 50 57.73	–40 15 22.3	2.21 ± 0.24
J225249-401256([b])			0.63 ± 0.13
J225344-401928	22 53 44.89	–40 19 27.2	2.17 ± 0.08

([a]) Low surface brightness flux present to the right of the source. Including it we get S = 4.3 mJy.
([b]) Coordinates are given only for Gaussian fitted sources. Fluxes for multi-component and/or low S/N sources were obtained by summing the pixels over the entire source.

4. Source variability

Before proceeding with the analysis of the radio spectral properties of our sample we should consider the possible effect of a

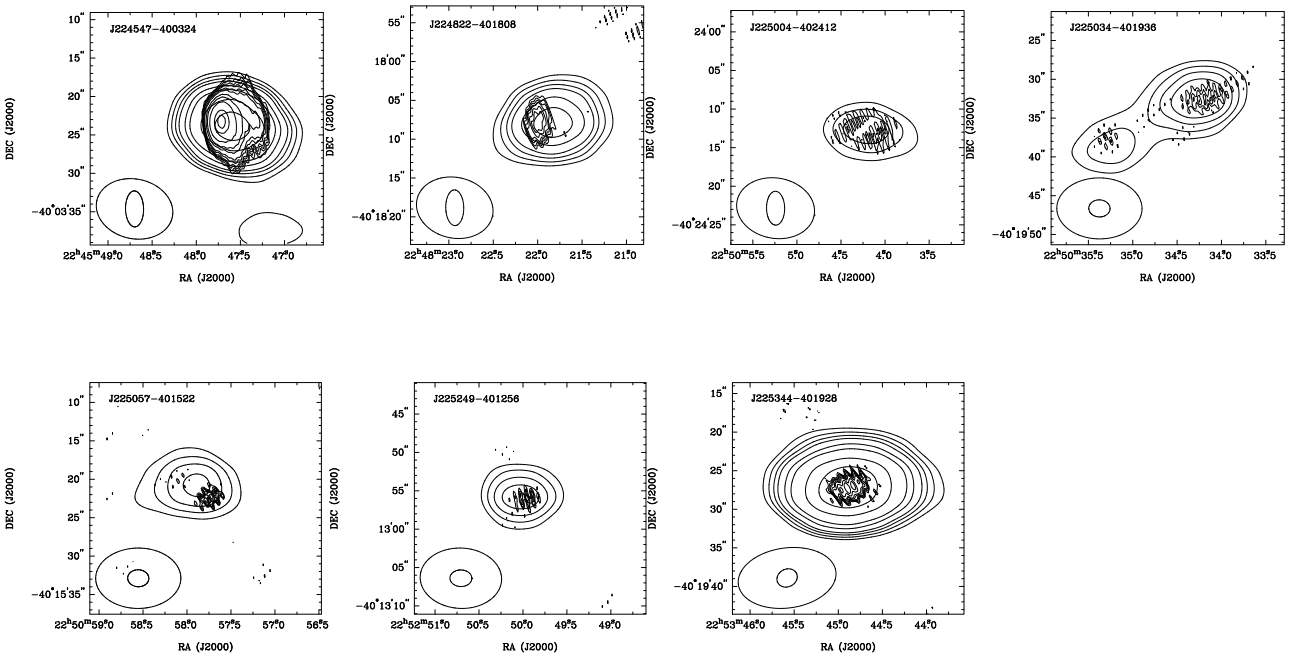

Fig. 2. *K*-band full resolution contours (thick lines) superimposed on low resolution contours (thin lines) for the seven sources detected in low resolution *K*-band images with $S/N > 6$. Contour levels are 3, 4, 5, 6, 8, 10, 15, 20, 30, 50 and 60% of the peak flux density.

source variability in shaping our radio spectra (presented later in Fig. 4). Although high frequency observations were done simultaneously in either 2007 or 2008, low frequency observations were done long before that, between 1994 and 2001.

From Sadler et al. (2006) we know that high frequency (*K*-band) variability is not very important on time scales of a few years: only 5% of the sources turn out to be variable at a level >30% over a baseline of 1−2 years. We assume that at the lower frequencies (1.4 and 4.8 GHz) the variability will be lower than that, since the low frequency emission may mostly come from extended, optically thin regions. However, we cannot exclude that in ten years time the overall level of emission at high frequencies has changed enough so that, for example, the spectral index $\alpha_{\rm M}$ (between 5 and 8.6 GHz) may have varied while $\alpha_{\rm L}$ (between 1.4 and 5 GHz) and $\alpha_{\rm H}$ (between 8.6 and 19 GHz) remained (roughly) constant. Such a change may manifest itself if, for example, both the high and low frequency spectral indices are negative, but the intermediate spectral index is positive. This kind of effect does indeed happen, as a visual inspection of Fig. 4 easily reveals (see e.g. sources J225057-401522 and J225404-402226), although it is not so big as to influence the discussion in a significant way. This confirms and strengthens the conclusion of Sadler et al. (2006) that strong source variability is a minor effect, even on time scales of the order of 5−10 years.

For a more quantitative analysis of the source variability in our sample, we compared the original ATESP 5 GHz fluxes (obtained in 2000/2001, see Prandoni et al. 2006) with the ones obtained with the 2007/2008 follow-up and checked the significance of their variations through the analysis of the so-called *variability index*. In particular we analysed two well-known variability indices, defined as follows (see Gregorini et al. 1986; Quirrenbach et al. 1992):

$$V_1 = \Delta S/\sigma_{\rm tot}$$
$$V_2 = \Delta S/\langle S \rangle$$

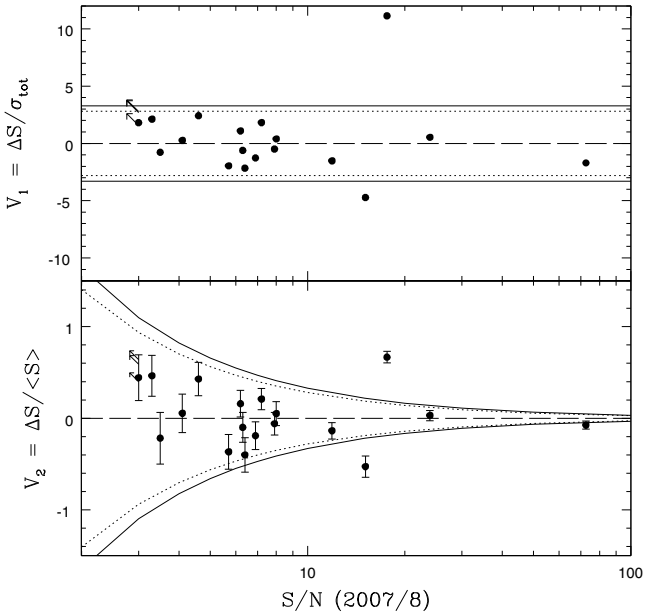

Fig. 3. Variability index V_1 (*Top*) and V_2 (*Bottom*) for single-component sources as a function of S/N (referred to 2007/8 observations). Arrows indicate sources which were not detected in epoch 2. Dotted and solid lines correspond to random ΔS fluctuation probabilities of 0.5% and 0.1% respectively.

where $\Delta S = S_1 - S_2$, with S_1 and S_2 being the 5 GHz fluxes measured respectively in epochs 1 (2000/01) and 2 (2007/08); $\sigma_{\rm tot} = \sqrt{\sigma^2(S_1) + \sigma^2(S_2)}$, and $\langle S \rangle = \frac{S_1+S_2}{2}$. We notice that V_2 represents the so-called *modulation index* as it reduces in the case of two epochs measurements.

Figure 3 shows the V_1 and V_2 variability index distribution as a function of the signal-to-noise ratio for single-component

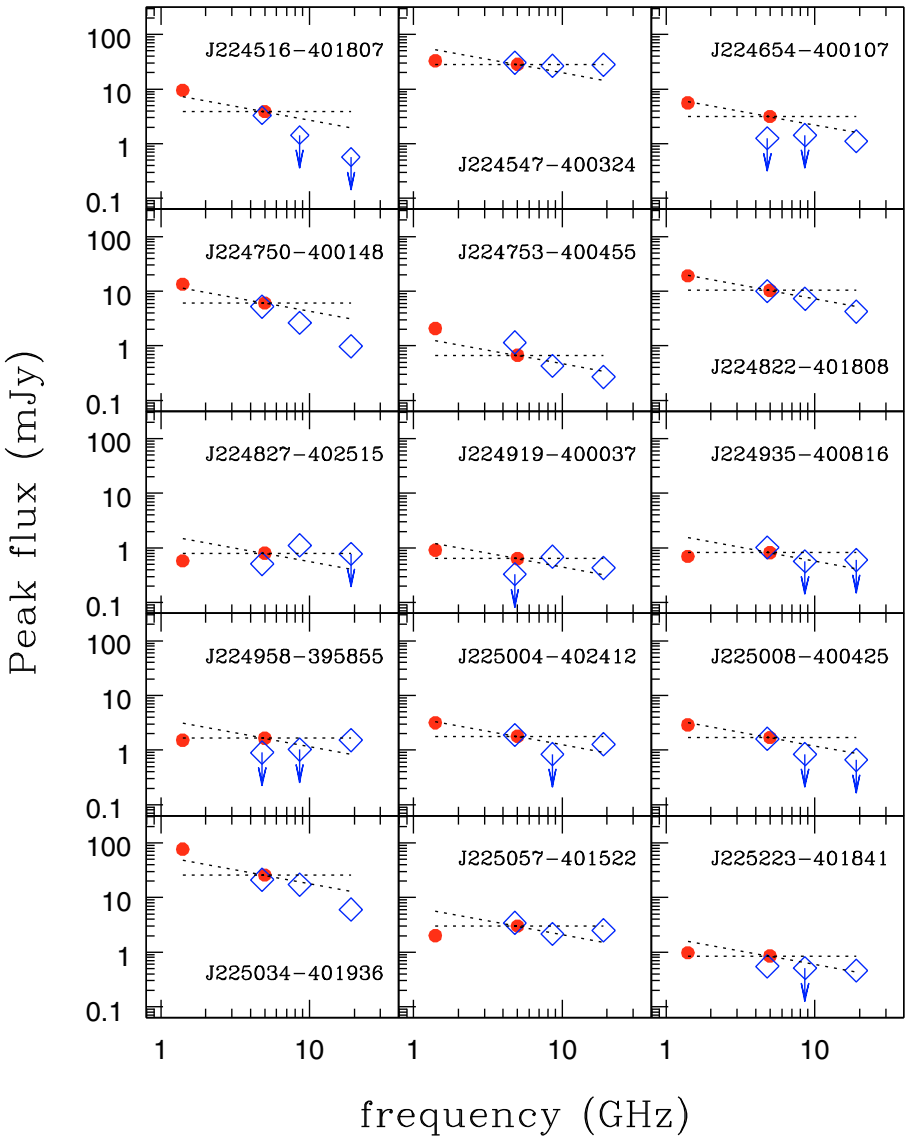

Fig. 4. Flux densities (in mJy) against frequency (in GHz) for the 26 ATESP 5 GHz sources associated to early-type galaxies discussed in this work (see Table 1). Red filled circles represent the original 1.4 and 5 GHz points (Prandoni et al. 2000b; Prandoni et al. 2006), while blue diamonds represent the 2007 and 2008 observations discussed in the present paper. No error bars are drawn, since these are typically smaller than symbols. Dotted lines indicate the expected slopes for $\alpha = 0$ and $\alpha = -0.5$.

sources (multi-component sources are unlikely to vary). To compute V_1 we estimated $\sigma(S_1)$ and $\sigma(S_2)$ through Condon's master equations (Condon 1997) by assuming calibration errors of the order of 3% for both epochs (see Prandoni et al. 2000b). Dotted and solid lines in Fig. 3 correspond to random Gaussian ΔS fluctuation probabilities of 0.5% and 0.1% respectively. In general a source is considered as a good *variable* candidate whenever the above probability is <0.1% (or $\Delta S > 3.29\sigma_{\rm tot}$). It is clear from the figure that two sources (J224753-400455 and J225344-401928) satisfy both the V_1 and V_2 variability criteria, while a third source (J224547-400324) is defined as *variable* only with respect to V_2 and for this reason has to be considered a less reliable candidate. All the other sources have 5 GHz flux variations consistent with being random fluctuations.

From the analysis of the overall source spectra (see Fig. 4) we see that source J224753-400455 ($\Delta S = -4.7\sigma_{\rm tot}$; $\Delta S = -0.53\langle S\rangle$) has a smooth power-law spectrum from 1.4 to 19 GHz, with the only exception of the 5 GHz point obtained in 2008. This argues against variability for this sources. On the other hand source J225344-401928 ($\Delta S = 11.1\sigma_{\rm tot}$; $\Delta S = 0.67\langle S\rangle$), clearly shows a change in the spectral shape from strongly inverted to flat when we go from the ATESP non-simultaneous flux measurements (red squares) to the present quasi-simultaneous flux determinations (blue diamonds). This strongly supports the hypothesis of variability. Source J224547-400324 is a less reliable candidate ($\Delta S = -1.7\sigma_{\rm tot}$) and flux variations, if real, are quite small ($\Delta S = -0.08\langle S\rangle$). The overall spectrum is rather flat over the entire frequency range covered. Both the flatness of the spectrum and the radio morphology (not inconsistent with a core-jet structure, see Fig. 2) may support the presence of some level of variability in this source.

In summary, we find that one of the 21 (e.g. 5%) single-component sources in our sample is a strong variable, while a second source may present some low-level variability. This is consistent with previous results. Tingay et al. (2003) found that the level of variability of powerful (~1 Jy), compact radio sources moderately increases with frequency from a median variability of 6% at 1.4 GHz to 9% at 8.6 GHz over a timescale of 3–4 years. Barvainis et al. (2005) found similar variability levels at 8.5 GHz for a sample of radio-loud and radio-quiet QSOs observed with the Very Large Array. It is worth noting that the flux density levels probed by the radio-quiet QSOs of the Barvainis et al. sample are similar to the flux densities of our sources ($\lesssim$1 mJy).

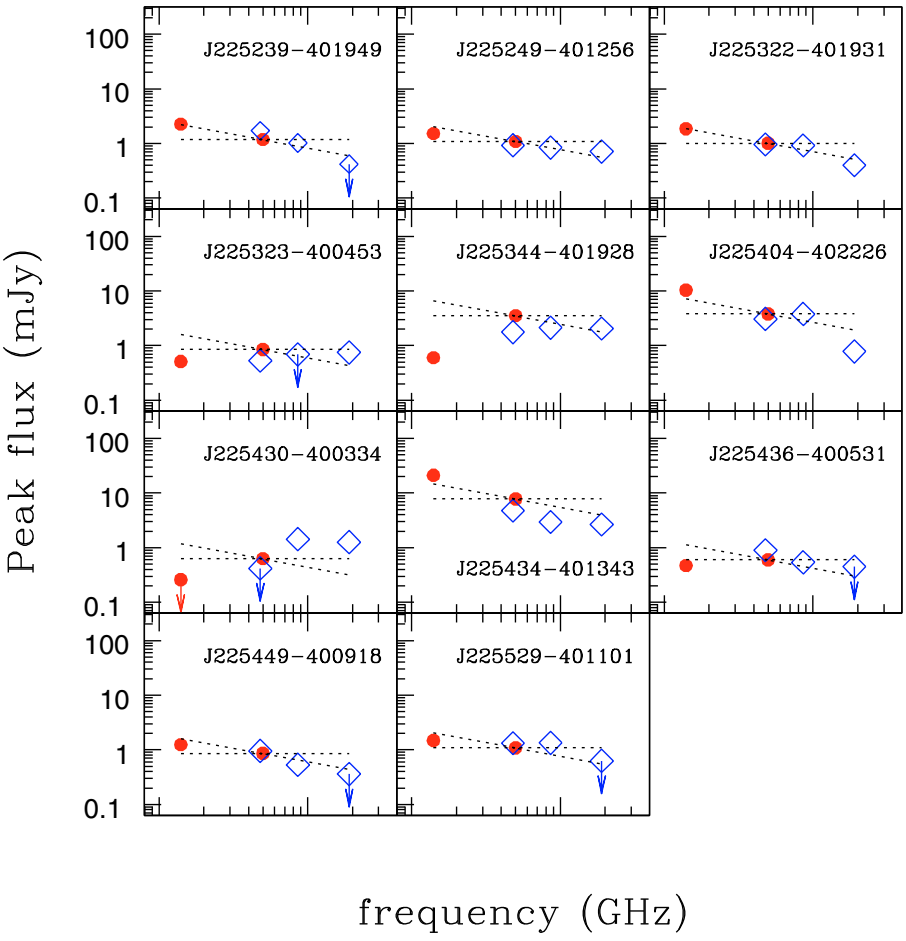

Fig. 4. continued.

5. Discussion of radio spectra

As already anticipated, Fig. 4 shows the overall radio spectra of the 26 ATESP 5 GHz sources associated with early-type galaxies discussed in this work. Red circles represent non-simultaneous ATESP 1.4 and 5 GHz observations, while blue diamonds represent the new quasi-simultaneous observations at 4.8, 8.6 and 19 GHz. We notice that low frequency spectral behaviour (steep or flat) derived from 1.4 and 5 GHz ATESP data is generally confirmed by high frequency simultaneous observations. This can be considered as a first qualitative confirmation of the fact that the sub-mJy flat-/inverted-spectrum population associated with early-type galaxies revealed by the ATESP 1.4 and 5 GHz surveys (Prandoni et al. 2006; Mignano et al. 2008) and discussed in Sect. 1 is genuine. The most notable exception is represented by the *variable* source J225344-401928 (see Sect. 4), which is remarkably characterised by a very inverted spectrum between 1.4 and 5 GHz ($\alpha_{\rm L} = 1.4$), not confirmed as real by high frequency simultaneous observations ($\alpha_{\rm M} \sim \alpha_{\rm H} \sim 0$).

For a more detailed analysis of the radio spectra we will focus below on two spectral indices, $\alpha_{\rm L}$ and $\alpha_{\rm H}$ (listed in Table 4). These two spectral indices can be used in a sort of "two-colour" diagram as was done in previuos works (see Sadler et al. 2006; Massardi et al. 2008; Tucci et al. 2008). Note that the analysis of the two-colour diagram is not exhaustive, and the spectral index between 4.8 and 8.6 GHz (e.g. $\alpha_{\rm M}$) may give further independent information on the spectrum, as previously noted in Sect. 4.

We will also compare our data with recent high frequency surveys (Sadler et al. 2006; Massardi et al. 2008; Tucci et al. 2008) and will try to determine how and to what extent frequency selection and flux limits influence the results. The ATESP 5 GHz survey is the only one selected at low frequency, while the other three are based on 20−30 GHz observations. Also there is quite a difference in the flux limit, which reaches from ∼0.6 mJy (our sample) via 20 mJy at 33 GHz (Tucci et al. 2008), 100 mJy at 20 GHz (Sadler et al. 2006) to 500 mJy at 20 GHz (Massardi et al. 2008). One extra selection criterion used for our sample was that we followed-up at high frequencies only sources associated with galaxies having early-type spectra; for that reason we also defined a sub-sample of 36 sources associated with galaxies from the Bright Source Sample discussed by Massardi et al. (2008). Since the latter sources are all bright in the radio, these are presumably all classical radio galaxies; their typical radio powers put most of them effectively in the FRII range.

Figure 5 shows two-colour diagrams of our (red symbols) and the Massardi et al. galaxy (blue diamonds) samples. Also plotted are all sources from the Massardi et al. sample that are associatd with quasars or quasar candidates (blue dots). We divided the sources in a nearby ($z < 0.5$, left panel) and a far ($z > 0.5$, right panel) sample, in order to check if distance may have an effect upon the spectral indices. In the far sample we included quasar candidates with unknown redshift, the large majority of which (presumably) are at redshifts >0.5 on the basis of their optical magnitude distribution.

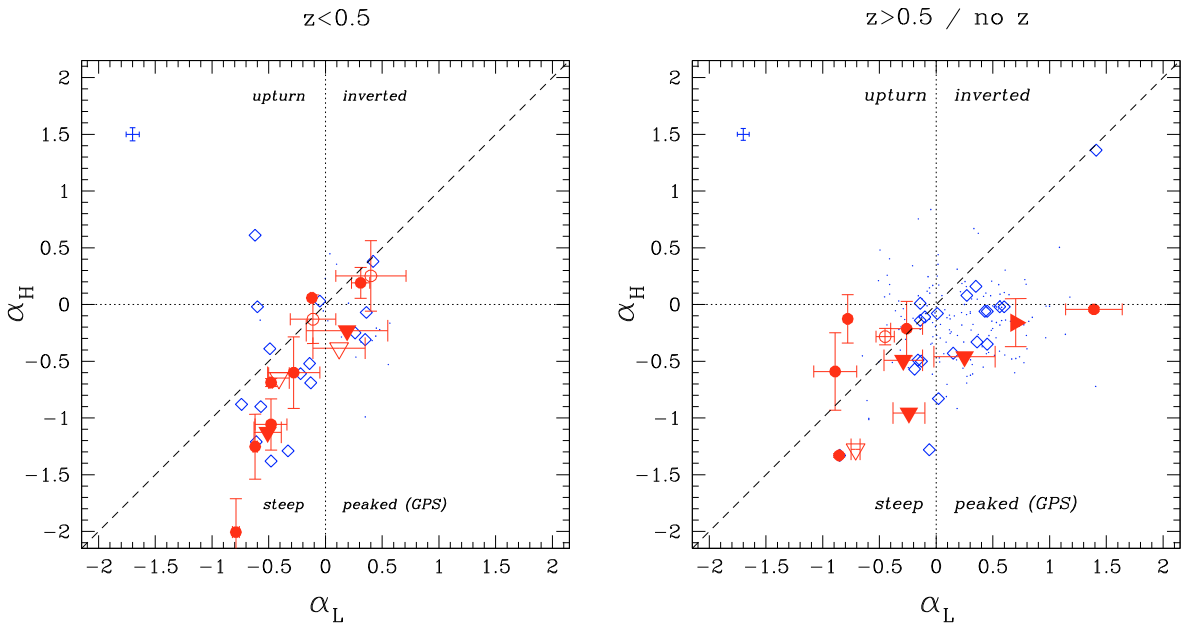

Fig. 5. High- against low-frequency spectral index. Red symbols indicate ATESP sources: filled symbols are used for α_H derived between 8.6 and 19 GHz and empty symbols are used for α_H derived between 4.8 and 19 GHz; triangles indicate upper/lower limits in α_H/α_L respectively. Blue diamonds indicate sources associated with early type optical spectra from the Massardi et al. (2008) sample; blue dots indicate sources associated with quasars or quasar candidates in the Massardi et al. (2008) sample. The typical error box for the Massardi et al. sources is indicated in the upper left corner. *Left panel*: objects with redshift <0.5. *Right panel*: objects with either redshift >0.5, or unknown redshift. The dashed line represents the location of sources with power-law spectra (i.e. with $\alpha_H = \alpha_L$). Horizontal and vertical dotted lines respectively indicate the $\alpha_H = 0$ and $\alpha_L = 0$ lines defining the four quadrants discussed in the text.

For a physical interpretation of the two-colour diagram we divided it in four quadrants, as done in previous works: 1) sources with $\alpha_L < 0$, $\alpha_H < 0$, conventionally named *steep*[1]; 2) sources with $\alpha_L < 0$, $\alpha_H > 0$, named *upturn*; 3) sources with $\alpha_L > 0$, $\alpha_H > 0$, named *inverted*; 4) sources with $\alpha_L > 0$, $\alpha_H < 0$, named *peaked*. We point out that the radio spectral index of the overall synchrotron emission from a jet-dominated radio source is expected to be from steep to moderately inverted ($-0.7 < \alpha < 0.2$) at the frequencies of this work, depending on the relative contributions of extended (optically-thin) and base (self-absorbed) jet components. Jet-dominated sources are therefore expected to mostly fall into the *steep* quadrant. Instead, for an ADAF, one expects $0.2 < \alpha < 1.1$ up to mm wavelengths (see Nagar et al. 2001), with α varying according to the accretion rate (f.i. $\alpha = 0.4$ when $L \sim 10^{-4} L_{\rm Edd}$ and $\alpha \sim 1$ when $L \leq 10^{-7} L_{\rm Edd}$; Mahadevan 1997). ADAF systems are therefore expected to fall into the *inverted* quadrant. Co-existence of moderate outflows can flatten the spectrum (with α remaining positive), whereas strong outflows can shift the peak of the radio emission from mm to cm wavelengths (Quataert & Narayan 1999).

As can be seen in Fig. 5 our ATESP sources, as well as the sources from the much brighter Massardi et al. galaxy sample, are mostly located in the lower part of the plots: 23/24 and 33/36 sources for the ATESP and the Massardi sample respectively have $\alpha_H < 0.2$. Although these numbers are significant only at about the 3σ level due to the relatively poor statistics involved, there can be little doubt that both samples consistently contain more sources with $\alpha_H < 0.2$. This is of course hardly surprising for the ATESP sample, which was originally selected at 5 GHz, but the high frequency selection of the Massardi sample does not make much difference, at least in this respect.

[1] In fact in this quadrant fall both steep ($\alpha < -0.5$) and flat ($-0.5 < \alpha < 0$) sources.

Less obvious a priori is the general steepening ($\alpha_L > \alpha_H$) of the spectra from low to high frequency. This is evident from the large number of sources lying below the diagonal dashed line, corresponding to power-law spectra (19/24 and 31/36 for ATESP and Massardi). These numbers are significant only at the 2σ level, but again both samples behave consistently and actually appear to cover identical regions in the two-colour diagram. Both facts favour a jet-dominated scenario, with steep-spectrum ($\alpha_H < -0.5$) sources dominated by synchrotron optically-thin emission and flat-spectrum ($\alpha_H > -0.5$) sources dominated by synchrotron optically-thick emission coming from the base of the jet. Nevertheless jet+ADAF models can also be consistent with values $0 \lesssim \alpha_H \lesssim 0.2$. Pure ADAF models ($\alpha_L$ and $\alpha_H \geq 0.2$) are ruled out by the present data (only one object in the Massardi galaxy sample can be considered as a pure ADAF candidate), indicating that such radiatively inefficient accretion regimes must be very rare also at the sub-mJy levels probed by the ATESP 5 GHz sample.

For a more quantitative analysis of the two-colour diagram we statistically compared both the low- and high-frequency spectral index distribution of the ATESP and the Massardi et al. galaxy samples by implementing the survival analysis methods described in Feigelson & Nelson (1985) and Isobe et al. (1986). This allows us to properly treat upper/lower limits in α_H/α_L respectively. Both α_L and α_H spectral index distributions of the ATESP and Massardi et al. samples are consistent with being drawn from the same parent population. In fact this hypothesis is rejected at only a $<2\sigma$ confidence level (Peto & Prentice generalized Wilcoxon test; Isobe & Feigelson 1990). This is especially interesting when we consider that the ATESP and the Massardi et al. samples cover very different ranges in flux density (by two or three orders of magnitude).

A similar comparison can be made between galaxies and quasars. To improve our statistics we consider the ATESP and

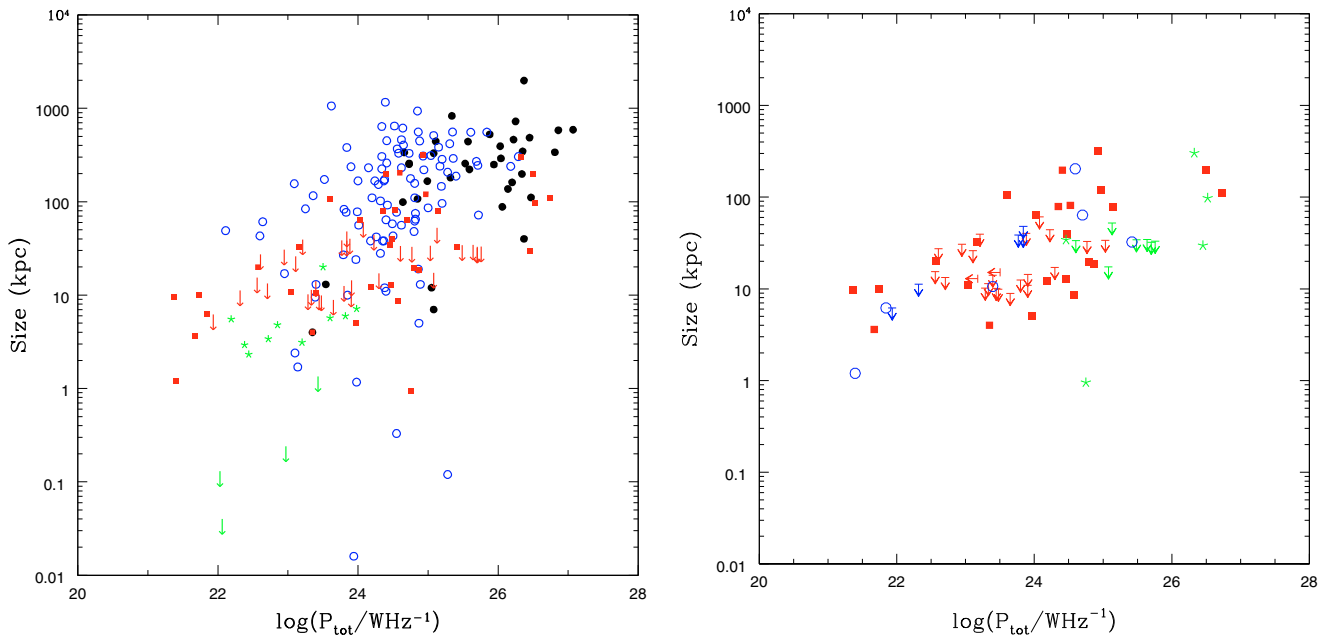

Fig. 6. Linear size as a function of radio power (at 1.4 GHz). *Left panel*: comparison between four different samples: ATESP 5 GHz sample (red squares and upper limits), B2 catalogue (blue open circles), 3C catalogue (black filled circles), radio-quiet QSO (green asterisks and upper limits). For Leipski et al. radio-quiet QSO sample 1.4 GHz luminosities were derived from tabulated 5 GHz values, assuming $\alpha = -0.7$. *Right panel*: comparison between different types of objects in the ATESP 5 GHz sample: sources associated to early type galaxies (red squares and upper limits); sources associated to late type galaxies (blue open circles and upper limits; among late type sources we may also have some mis-classified narrow-line AGN); sources associated to broad-line AGNs, typically quasars (green asterisks and upper limits).

Table 6. Mean values and standard deviations of the low and high frequency spectral indices.

Sample[(a)]	α_L	σ	α_H	σ
ATESP	−0.18	(0.11)	−0.79	(0.16)
Massardi G	−0.01	(0.08)	−0.35	(0.09)
ATESP + Massardi G far	−0.08	(0.07)	−0.50	(0.08)
Massardi Q far	0.21	(0.04)	−0.16	(0.03)

[(a)] "Massardi G" and "Massardi Q" respectively refer to galaxies and stellar identifications of the Massardi et al. sample. "Far" refers to $z >$ 0.5 sources (or unknown redshift for quasar candidates).

Table 7. Spectral type statistics in five samples[(a)].

	ATESP >0.6 mJy (percent)		M-G >500 mJy (percent)		Tuc >20 mJy (percent)		Sad >100 mJy (percent)		M >500 mJy (percent)	
U	9	±5	8	±5	29	±6	22	±5	10	±1
I	13	7	12	6	7	3	20	4	28	5
S	61	14	47	11	53	7	34	6	30	5
P	17	8	33	11	11	3	24	5	32	5

[(a)] ATESP 5 GHz sample (26 sources); Massardi et al. galaxy sample (M-G, 36 sources); Tucci et al. (2008) sample (Tuc, 102 sources); Sadler et al. (2006) sample (Sad, 101 sources) Massardi et al. (2008) overall sample (M, 218 sources).

the Massardi et al. galaxies as a single population, and we limit our analysis to $z > 0.5$ sources, where most quasars (or quasar candidates) are located (see right panel of Fig. 5). In this case we find that the hypothesis that $z > 0.5$ galaxies and quasars are extracted from the same parent population is rejected at a $>4.5\sigma$ level (Peto & Prentice generalized Wilcoxon test; Isobe & Feigelson 1990). Table 6 summarises the mean values for the samples discussed above (Kaplan-Meier estimator, Isobe & Feigelson 1990). We notice that the Massardi sub-sample of $z > 0.5$ quasars and quasar candidates (Massardi Q far) tend to be flatter or even more inverted than sources associated with galaxies, indicating that quasar-like objects are more commonly associated with compact sources and less with the classical extended radio lobes in which the optically thin synchrotron radiation with steep radio spectra is dominant. On the other hand, no difference is seen in spectral steepening: if we compare the curvature $C = \alpha_H - \alpha_L$ (see e.g. Gregorini et al. 1984), we find $C = -0.42 \pm 0.11$ (ATESP + Massardi G far), and $C = -0.37 \pm 0.05$ (Massardi Q far).

Following Sadler et al. (2006) we consider in more detail the distribution of sources in the four quadrants of the two-colour diagram, which represent different types of radio sources (defined earlier in this section). The distribution of objects over the four quadrants is shown in Table 7 (where U stands for *Upturn*, I for *Inverted*, S for *Steep*, P for *Peaked*). Most ATESP sources are in the lower left quadrant (61%, Table 7), as for classical FRI and FRII radio galaxies. This may be due to the early type galaxy optical pre-selection, and in fact the entries of the Massardi et al. galaxy sample (M-G in Table 7) are, considering the errors, practically the same as those of the ATESP sample, despite the very different flux range covered by the two samples.

In Table 7 we also compare the distribution of objects in three samples, all selected at high (≥20 GHz) frequencies, where no optical pre-selection was applied (Tucci et al. 2008; Sadler et al. 2006; Massardi et al. 2008). There appear to be some trends with flux density, which we can attribute partly to selection effects and partly to the different composition of the overall samples, in which quasar spectra may be more or less dominant, depending on the limiting flux density. The *upturn* and *steep* spectra (i.e. the left hand side of the two-colour diagram) tend to become more numerous at lower flux densities, while the inverse happens with *inverted* and *peaked* spectra (right hand side). These trends are individually significant only at the 2σ level, again due to the small numbers involved, but appear to be quite

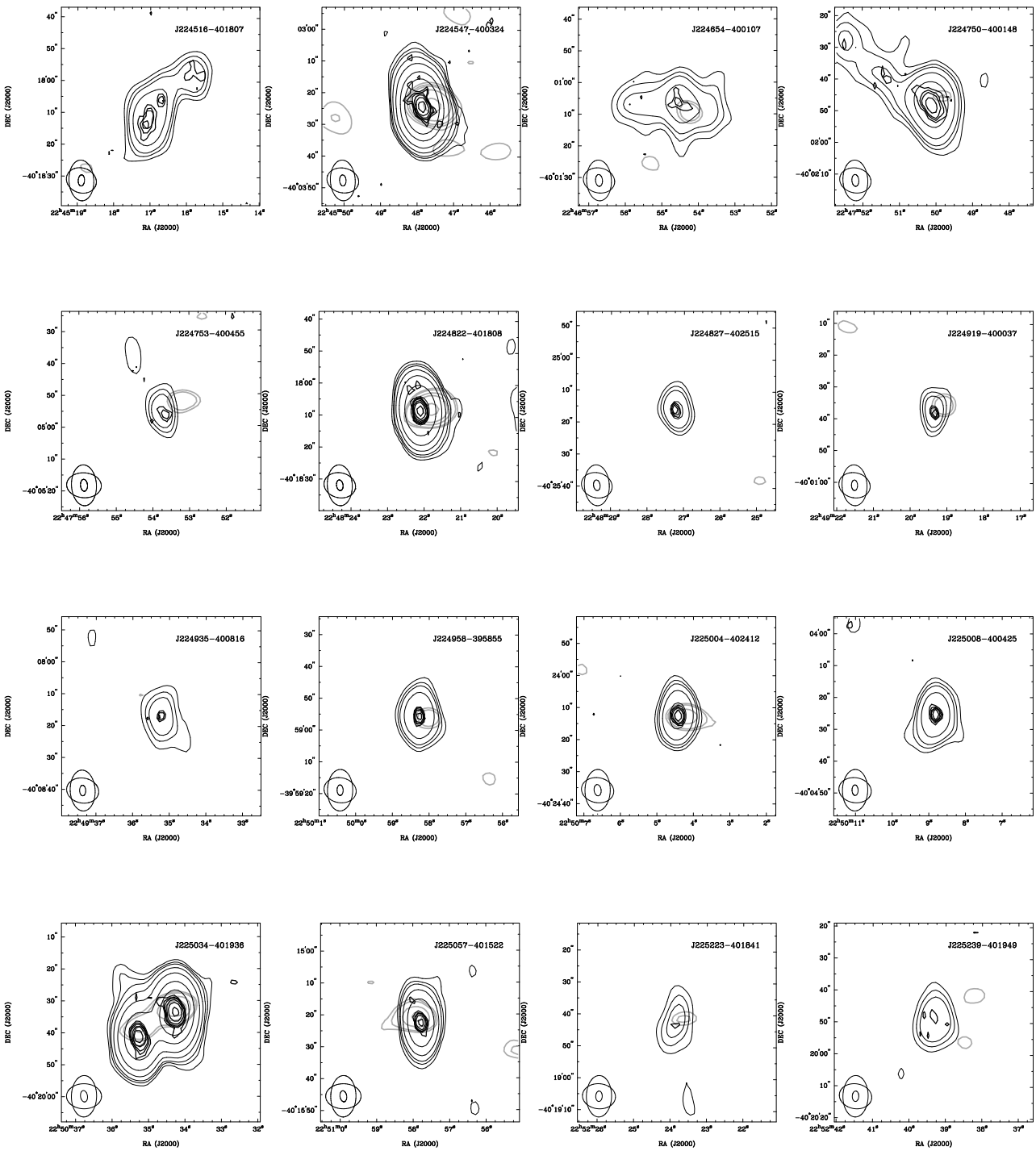

Fig. 7. Contour images of the 26 ATESP 5 GHz sources identified with early-type galaxies, discussed in this work. Thin black contours represent low resolution 5 GHz data; superimposed are high resolution 5 GHz contours (thick black lines) and low resolution K-band contours (thick gray lines). Contour levels are 2.5 (only K-band), 3, 4.5, 6, 10, 20, 50 and 100% of the peak flux density.

consistent in all four quadrants. If we sum the U and S sources (those with $\alpha_{\rm L} < 0$) and the I and P sources ($\alpha_{\rm L} > 0$), the dependence on the flux density becomes quite obvious: whereas about 18% of the sources have a positive $\alpha_{\rm L}$ (I and P) at the flux density level of the Tucci et al. (2008) sample, at the much higher flux levels of the Massardi et al. sample this strongly increases to about 60%; this difference is definitely significant at about 4σ. The fact that the number of rising spectra increases with flux limit was already noticed by Bolton et al. (2004). No doubt these trends may be due to selection effects; however, the possible increase of *peaked* sources at higher flux densities is harder to explain by selection effects only.

6. The AGN component of the ATESP 5 GHz sample

In Sect. 5 we discussed the radio spectral properties of a representative sub-sample of ATESP radio sources associated to early type galaxies in comparison with some recent high-frequency radio surveys. The main results of such an analysis can be summarised as follows. Most sources have spectra ranging from

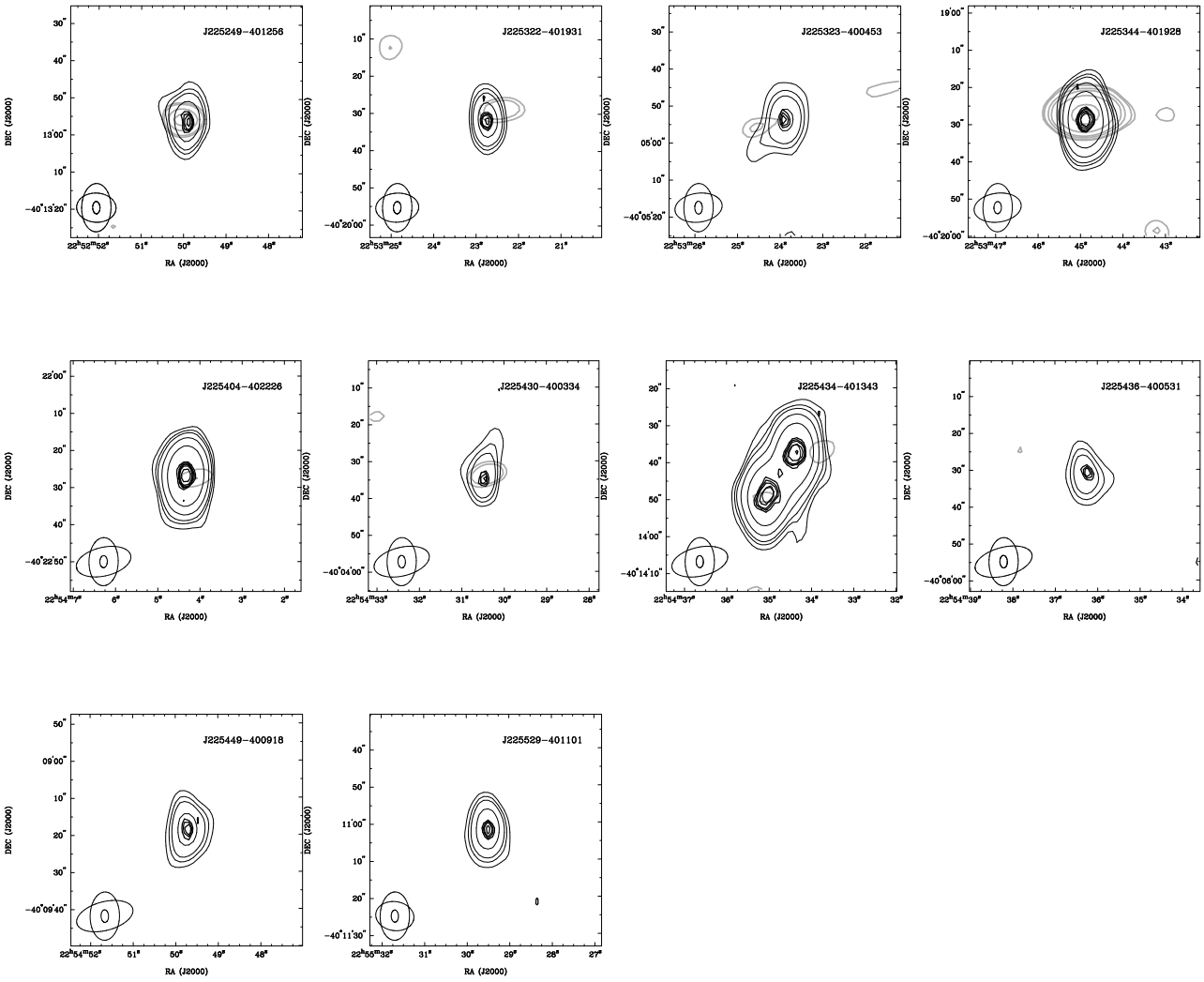

Fig. 7. continued.

steep to moderately inverted, which is consistent with them being jet-dominated systems. Strong spectral similarities found between our and the much brighter Massardi et al. galaxy sample may suggest that our radio sources are simply lower luminosity counterparts of FRII radio galaxies. No evidence for an ADAF population was found, and *peaked* GPS-like sources seem to be preferentially found at higher flux densities than the ones probed by the ATESP. In addition quasar-like *upturn* sources are rare ($9 \pm 5\%$, see Table 7). While this latter result is partly a consequence of the ATESP optical pre-selection, it argues against an obscured radio-quiet quasar population hidden among the ATESP early type galaxies. Nevertheless compact quasar-like objects may be present among flat/moderately inverted jet-dominated sources.

To further explore this hypothesis and probe the AGN component of the ATESP sample at large we now compare linear sizes and radio powers of all the ATESP sources with redshift determination (71 sources, see Table 1), with the ones of the well-known B2 (Colla et al. 1975; Fanti et al. 1978) and 3CR (Laing et al. 1983) radio source catalogues, and with sizes and powers of a sample of optically-selected radio-quiet QSO (Leipski et al. 2006). B2 and 3C catalogues probe different ranges in radio luminosity, with the former dominated by FRI ($P < 10^{25}$ W/Hz) and the latter by FRII ($P > 10^{25}$ W/Hz) radio galaxies. Such a comparison is shown in Fig. 6 (left panel). In the right-hand panel of Fig. 6 the same plot is shown, where symbols now stand for different optical types of ATESP radio sources.

We first focus our analysis on ATESP resolved sources (red squares in left panel). Such sources have generally larger sizes than radio-quiet QSOs and seem to be more consistent with the B2 radio galaxy size distribution. In particular they seem to confirm and extend to lower radio luminosity the size-power relation found for B2 radio galaxies (de Ruiter et al. 1990). When enlarging the analysis to unresolved sources (red upper limits in left panel), we notice a group of sources at $P > 10^{25}$ W/Hz which clearly stand below the B2/3C source size distribution. As shown in the right panel of Fig. 6, such sources are in fact associated to broad-line AGNs (see green upper limits) and could be genuine compact sources, perhaps the radio-intermediate counterparts of radio-quiet QSOs. Unresolved sources with radio powers $P < 10^{25}$ W/Hz are mostly associated to early-type galaxies. In general the given upper limits do not allow us to distinguish between B2 FRI-like and quasar-like sizes. Nevertheless in some cases we have $d \lesssim 10$ kpc, making such sources more consistent with a radio-quiet scenario. Some of those sources may also be low power BL Lac, where the optical activity is very weak (see discussion in Sect. 1). From geometrical considerations we expect <3−6% (or <2−4) of such objects in the sample, assuming viewing angles <15°−20° (Zenzus & Pearson 1987). Such fraction could be somewhat higher, due to possible sample

contamination from boosted objects belonging to a parent population fainter than the ATESP flux limit. For a more conclusive analysis of the size-power plot we need higher resolution data for the ATESP sample. In particular VLBI imaging would allow us to better probe the low power BL Lac scenario. As a final remark it is worth noticing that ATESP source sizes may suffer from some underestimation. This because low surface brightness flux associated to radio jets could be missed by blind source Gaussian fitting procedures performed to construct the ATESP source catalogues (see Prandoni et al. 2000b, 2006).

7. Summary

We presented follow up quasi-simultaneous observations at 4.8, 8.6 and 19 GHz for a representative sub-sample of ATESP sources associated to early type galaxies (26 sources with $S > 0.6$ mJy). The new data were discussed together with the original 1.4 and 5 GHz ATESP data (Prandoni et al. 2000b, 2006), with the aim of better understanding the radio spectral properties of such sources and ultimately the nature of AGNs at sub-mJy flux levels. In particular we were interested in understanding whether the AGN component of the sub-mJy population is more related to efficiently accreting systems – like radio-intermediate/quiet quasars – or to systems with low accretion rates – like e.g. FRI radio galaxies – or to low radiative efficiency accretion flows – like e.g. ADAF.

From the analysis of the radio spectra, we found that our sources are most probably jet-dominated systems, with steeper sources dominated by optically-thin synchrotron emission (typical of FRI and FRII radio galaxies) and flatter or moderately-inverted sources dominated by optically-thick emission coming from the base of the jet. Pure ADAF models seem to be ruled out by the high frequency data, while ADAF+jet scenarios could be consistent with flat/moderately inverted sources, but are not required to explain the data.

By comparing our sample with some recent high frequency ($\gtrsim$20 GHz) surveys we found strong spectral similarities between our and the much brighter Massardi et al. galaxy sample, possibly suggesting that our radio sources are mostly lower luminosity counterparts of the Massardi et al. (FRII) radio galaxies. In addition *peaked* GPS-like sources seem to be preferentially found at higher flux densities than the ones probed by the ATESP sample, and quasar-like *upturn* sources are rare ($9 \pm 5\%$). This latter result is partly due to the ATESP early type galaxy pre-selection, but argues against an obscured radio-quiet quasar population hidden among the ATESP early type galaxies. Nevertheless compact quasar-like objects may be present among flat/moderately inverted jet-dominated sources.

To further investigate such a hypothesis we compared radio powers and linear sizes of the ATESP 5 GHz sample with the ones of two well-known brighter radio source catalogues (B2 and 3CR) and with the sample of radio-quiet quasars studied by Leipski et al. (2006). Unfortunately such a comparison suffers from the large number of unresolved ATESP sources (or the large number of size upper limits). A significant fraction of ATESP sources have sizes consistent with the ones of B2 and 3CR radio galaxies. Such sources seem to confirm and extend to lower radio luminosity the size-power relation found for B2 radio galaxies (de Ruiter et al. 1990). On the other hand, a component of very compact $d < 10$ kpc radio sources associated to early type galaxies seem to have sizes more consistent with the ones of radio-quiet quasars. Among them we may have a few low power BL Lac. For a more conclusive analysis we need higher resolution (possibly VLBI) data for the ATESP sample.

Acknowledgements. The Australia Telescope Compact Array is part of the Australia Telescope which is funded by the Commonwealth of Australia for operation as a National Facility managed by CSIRO.

References

Abramowicz, M. A., Igumenshchev, I. V., Quataert, E., & Narayan, R. 2002, ApJ, 565, 1101
Afonso, J., Mobasher, B., Koekemoer, A., Norris, R. P., & Cram, L. 2006, AJ, 131, 1216
Barvainis, R., Lehar, J., Birkinshaw, M., Falcke, H., & Blundell, K. 2005, ApJ, 618, 122
Bolton, R. C., Cotter, G., Pooley, G. G., et al. 2004, MNRAS, 354, 485
Clark, B. G. 1980, A&A, 89, 377
Colla, C., Fanti, C., Fanti, R., et al. 1975, A&AS, 20, 1
Condon, J. J. 1984, ApJ, 287, 461
Condon, J. J. 1997, PASP, 109, 166
De Zotti, G., Ricci, R., Mesa, D., et al. 2005, A&A, 431, 893
Doi, A., Kameno, S., Kohno, K., Nakanishi, K., & Inoue, M. 2005, MNRAS, 363, 692
Falcke, H., & Biermann, P. L. 1999, A&A, 342, 49
Fanaroff, B. L., & Riley, J. M. 1974, MNRAS, 167, 31
Fanti, R., Gioia, I., Lari, C., & Ulrich, M. H. 1978, A&AS, 34, 341
Feigelson, E. D., & Nelson, P. I. 1985, ApJ, 293, 192
Georgakakis, A., Mobasher, B., Cram, L., et al. 1999, MNRAS, 306, 708
Giroletti, M., Giovannini, G., & Taylor, G. B. 2005, A&A, 441, 89
Gregorini, L., Mantovani, F., Eckart, A., et al. 1984, AJ, 89, 323
Gregorini, L., Ficarra, A., & Padrielli, L. 1986, A&A, 168, 25
Gruppioni, C., Ciliegi, P., Rowan-Robinson, M., et al. 1999, MNRAS, 305, 297
Isobe, T., & Feigelson, E. D. 1990, BAAS, 22, 917
Isobe, T., Feigelson, E. D., & Nelson, P. I. 1986, ApJ, 306, 490
Jarvis, M. J., & Rawlings, S. 2004, New Astron. Rev., 48, 1173
Hildebrandt, H., Erben, T., Dietrich, J. P., et al. 2006, A&A, 452, 1121
Högbom, J. A. 1974, A&AS, 15, 417
Klöckner, H.-R., Martínez-Sansigre, A., Rawlings, S., & Garrett, M. A. 2009, MNRAS, 398, 176
Lacy, M., Laurent-Muehleisen, S. A., Ridgway, S. E., Becker, R. H., & White, R. L. 2001, ApJ, 551, L17
Laing, R. A., Riley, J. M., & Longair, M. S. 1983, MNRAS, 204, 151
Leipski, C., Falcke, H., Bennert, N., & Hüttemeister, S. 2006, A&A, 455, 161
Magliocchetti, M., Maddox, S. J., Wall, J. V., Benn, C. R., & Cotter, G. 2000, MNRAS, 318, 1047
Mahadevan, R. 1997, ApJ, 477, 585
Massardi, M., Ekers, R. D., Murphy, T., et al. 2008, MNRAS, 384, 775
Mignano, A., Miralles, J.-M., da Costa, L., et al. 2007, A&A, 462, 553
Mignano, A., Prandoni, I., Gregorini, L., et al. 2008, A&A, 477, 459
Muxlow, T. W. B., Richards, A. M. S., Garrington, S. T., et al. 2005, MNRAS, 358, 1159
Nagar, N. M., Wilson, A. S., & Falcke, H. 2001, ApJ, 559, L87
Narayan, R., & Yi, I. 1994, ApJ, 428, L13
Nonino, M., Bertin, E., da Costa, L., et al. 1999, A&AS, 137, 51
O'Dea, C. P. 1998, PASP, 110, 493
Olsen, L. F., da Costa, L., Madejsky, R., et al. 2006, A&A, 456, 881
Prandoni, I., Gregorini, L., Parma, P., et al. 2000a, A&AS, 146, 31
Prandoni, I., Gregorini, L., Parma, P., et al. 2000b, A&AS, 146, 41
Prandoni, I., Gregorini, L., Parma, P., et al. 2001a, A&A, 365, 392
Prandoni, I., Gregorini, L., Parma, P., et al. 2001b, A&A, 369, 787
Prandoni, I., Parma, P., Wieringa, M. H., et al. 2006, A&A, 457, 517
Quataert, E., & Narayan, R. 1999, ApJ, 520, 298
Quirrenbach, A., Witzel, A., Kirchbaum, T. P., et al. 1992, A&A, 258, 279
Ricci, R., Sadler, E. M., Ekers, R. D., et al. 2004, MNRAS, 354, 305
Richards, E. A., Fomalont, E. B., Kellermann, K. I., et al. 1999, ApJ, 526, L73
de Ruiter, H. R., Parma, P., Fanti, C., & Fanti, R. 1990, A&A, 227, 351
Sadler, E. M., Ricci, R., Ekers, R. D., et al. 2006, MNRAS, 371, 898
Sault, R. J., & Wieringa, M. H. 1994, A&AS, 108, 585
Smolcic, V., Schinnerer, E., Scodeggio, M., et al. 2008, ApJS, 177, 14
Snellen, I. A. G., Schilizzi, R. T., Miley, G. K., et al. 2000, MNRAS, 319, 445
Steer, D. G., Dewdney, P. E., & Ito, M. R. 1984, A&A, 137, 159
Tingay, S. J., Jauncey, D. L., King, E. A., et al. 2003, PASJ, 55, 351
Tucci, M., Rubino-Martin, J. A., Rebolo, R., et al. 2008, MNRAS, 386, 1729
Vettolani, G., Zucca, E., Merighi, R., et al. 1998, A&AS, 130, 323
Waldram, E. M., Bolton, R. C., Pooley, G. G., & Riley, J. M. 2007, MNRAS, 379, 1442
Zenzus, J. A., & Pearson, T. J. 1987, in Superluminal Radio Sources (Cambridge: Cambridge University Press), 1